Dynamic characterization of timber floors sub-assemblies: sensitivity analysis and modelling issues

Dag Pasquale Pasca[1], Angelo Aloisio[2], Massimo Fragiacomo[3], and Roberto Tomasi[4]

[1]Faculty of Science and Technology, Norwegian University of Life Sciences, Drøbakveien 31, 1433 Ås, Norway. Email: dag.pasquale.pasca@nmbu.no

[2]Department of Civil, Construction-Architectural and Environmental Engineering, Università degli Studi dell'Aquila, Via G. Gronchi 18, 67100 L'Aquila, Italy. Email: angelo.aloisio1@graduate.univaq.it

[3]Department of Civil, Construction-Architectural and Environmental Engineering, Università degli Studi dell'Aquila, Via G. Gronchi 18, 67100 L'Aquila, Italy. Email: massimo.fragiacomo@univaq.it

[4]Faculty of Science and Technology, Norwegian University of Life Sciences, Drøbakveien 31, 1433 Ås, Norway. Email: roberto.tomasi@nmbu.no

ABSTRACT

Timber floors are prone to exhibit vibration levels which can cause discomfort to the occupants. In the last twenty years, ambient vibration tests have become very popular due to the many advantages they have over traditional forced vibration tests, when dealing with civil engineering structures. Furthermore, sensitivity analyses and "black box" optimization algorithms can support the development of refined finite element models that accurately predict the structures' responses based on the experimental modal parameters. However, applications of these methods and techniques to timber structures are scarce compared to traditional materials. This paper presents and discusses the findings of an experimental testing campaign on a lightweight timber floor. At first, each component of the assembly was tested separately under different boundary conditions. Then

the authors evaluated the behaviour of the whole floor assembly. In a second step, the authors carried out a covariance-based sensitivity analysis of FE models representative of the tested structures by varying the different members' mechanical properties. The results of the sensitivity analysis highlighted the most influential parameters and supported the comparison between diverse FE models. As expected, the longitudinal modulus of elasticity is the most critical parameter, although the results are very dependent on the boundary conditions. Then automatic modal updating algorithms tuned the numerical model to test results. As a concluding remark, the experimental and numerical results were compared to the outcomes of a simplified analytical approach for the floor's first natural frequency estimate based on Eurocode 5.

INTRODUCTION

Modal testing represents a standard practice in structural engineering. Traditional modal testing is based on estimating frequency response functions, which basically are the ratio of the output response to the input excitation. This approach is also known as Experimental Modal Analysis (EMA). Other ways to obtain modal properties through testing are the so-called Operational Modal Analysis (OMA) methods. These approaches are very advantageous in civil engineering, where the tested object is usually massive.

OMA encouraged copious research activities, which spanned from theoretical investigations (Aloisio et al. 2020e; Reynders et al. 2012; Reynders et al. 2016) to practical applications (Bedon and Morassi 2014; Rainieri et al. 2019; Aloisio et al. 2020a; Aloisio et al. 2020c). The scientific literature documents a considerable amount of applications to civil engineering structures: wind turbines (Tcherniak et al. 2011; Devriendt et al. 2014), stadiums (Peeters et al. 2007; Magalhães et al. 2008), dams (Sevim et al. 2011; Pereira et al. 2018), architectural heritages (Kita et al. 2019; Gentile et al. 2019; Antonacci et al. 2020; Aloisio et al. 2020d). The modal features, obtained from OMA, bestow a direct insight into the actual structural behaviour and can guide a heedful assessment about the modelling of the tested structures. A high-quality experimental campaign can yield a reliable estimation of many modal parameters, valuable in understanding the limits and advantages of the possible modelling approaches. The matching between the experimental modal parameters and those obtained from the numerical model endorses the modelling choices. The search for an optimum matching leads to an optimum model, obtained by optimizing the modelling variables via the so-called model updating methods (Friswell and Mottershead 2013). Model updating defines the process of refreshing the modelling variables at each step to minimize a proper objective function, which magnifies the difference between experimental and numerical features. In the digital era, model updating is gaining popularity due to automated optimization algorithms. These algorithms lead to an optimum structural model, which best mirrors the experimental response. The increasing popularity of model updating methods has alimented considerable research. Today, a researcher can use numerous optimization algorithms, which are equally feasible in terms of reliability and computational efforts.

Timber is an excellent construction material with good stiffness-to-mass ratios and carbon-storing properties. These characteristics has made timber very popular in the last years. The interest in timber structures has risen, especially in the last two decades, due to the advent of new engineering wood products, like the Cross-Laminated Timber (Ceccotti et al. 2013; Brandner et al. 2016; Izzi et al. 2018; Aloisio et al. 2020b). The low weight of timber, however, is a double-edged sword to the dynamic performance. The use of timber elements is beneficial in reducing dead loads (and inertial forces) on the structure. On the other hand, its low mass makes it prone to reach a higher amplitude of vibrations. The assessment of timber buildings' vibration performances has two primary branches: one focused on evaluating the lateral response(Reynolds et al. 2016; Mugabo et al. 2019; Aloisio et al. 2020f; Aloisio et al. 2021), the other on assessing walk-induced vibrations and the comfort requirements for the users (Smith et al. 2007). While the first field is relatively new, researchers have investigated the second aspect for many years (Ohlsson 1982; Smith and Chui 1988; Hu et al. 2001; Hamm et al. 2010). The serviceability limit state is related to the perception of annoying oscillations caused by walking-induced vibrations. The "live" feel of timber floors is familiar to many, especially in single-family housing with a timber framework. However, this problem is not limited to timber-framed residential buildings. Timber joists can support the flooring system even in masonry buildings (Hu et al. 2001). The trend of seeking large, open-spaced architectural layout and adopting new construction practices certainly affects timber floors' serviceability significantly. The ability to predict timber flooring systems' behaviour remains a difficult task and a topical subject.

There are some applications of ambient vibration tests on timber floors in the scientific literature (Weckendorf and Smith 2012; Weckendorf et al. 2014; Weckendorf et al. 2016). However, force vibration tests, and EMA methods remain the most known and used procedures to estimate traditional floors' modal properties or more innovative solutions (e.g. CLT and Timber concrete composites) (Casagrande et al. 2018; Xie et al. 2020; Huang et al. 2020). Applications of OMA methods and automated modal updating procedures to timber structures are still not copious. This paper presents and discusses ambient vibration test results of a timber floor and the modelling strategies and techniques adopted to simulate the floor's dynamic response numerically. Specifically, the research studies the response of two glulam beams with plywood decking, which are part of a simply-supported timber floor. At first, each assembly component was tested separately under different boundary conditions; then, the authors evaluated the whole floor assembly's behaviour. In a second step, the authors carried out a covariance-based sensitivity analysis on the FE models representing the tested structures by varying the Moduli of Elasticity of the different members. The sensitivity analysis outcomes evidence the significant structural parameter and drive a definitive comparison between diverse FE modelling methods. The authors used two automated updating algorithms to refine the numerical model's parameters better and match the testing results. The adoption of closed-form analytical solutions is diffuse in engineering practice. Therefore, the authors compared the well-known Euler-Bernoulli model for the simply-supported beam tests with the FE numerical predictions.

MATERIALS AND METHODS

The authors tested a timber floor sub-assembly made by two beams and decking above. The two GL30C beams are 5m long with a 115mm x 315mm cross-section. The nominal average Modulus of Elasticity (MoE) is $13GPa$, while the mean weight is $430kg/m^3$, according to EN

14080 (EN14080 2013). Both beams presented some defect at delivery, see Fig1. "Beam 1" on one end had two cracks (approximately 15cm and 20cm wide), on both faces; while "Beam 2" had a hole on one face that was filled with silicone.

The decking consists of 21 mm thick Plywood 1,5 x 1,5 m sheets made from Birch veneers. According to the producer declaration of performance (DoP) the self-weight is $650kg/m^3$, while the mean values of the MoE span between $6GPa$ and $8GPa$, depending on loading direction, perpendicular or parallel to the external layer fibre orientation, respectively.

In modal testing practice, mechanical parts, machinery and other structural components are tested freely-suspended due to the difficulties in modelling the boundary conditions. Due to the laboratory conditions, it was not possible to suspend the beams. The authors adopted a compromise solution, based on the use of a layer of Rockwool insulation placed under the beams, which successfully simulated the free-free boundary conditions. A single rectangular piece of Rockwool (300mm x 300mm, 100mm thick) located under the mid-span of the beams, or by the centre of the plywood boards yielded the best results, in terms of repeatability, consistency and clearness of both the spectral densities and the stabilisation diagrams. The presence of the Rockwool layer may affect the results in terms of damping. However, reliable damping estimates are always challenging to achieve and are not the primary scope of this investigation.

Pinned-pinned boundary conditions characterized the floor assembly in Fig2. Two metal cylinders, spaced 4.8m, supported each beam, with a 600mm centre-to-centre distance. The decking was made of three square boards with 1.5m long sides. The beams, being 5m long, were not covered by the boards for the last 25cm on each side, see Fig2a. Furthermore, no nailed or screwed connector secured the boards over the beams. Dynamic analyses are susceptible to the occurrence of little damage or minimal structural modification. The insertion of the connectors would have altered/damaged each component, thus nullify the efforts to identify the dynamics of each of them accurately. Therefore, the authors devised an alternative solution to study the entire structural arrangement without the need for connectors. They placed a reusable putty-like pressure-sensitive adhesive, which guarantees the joint response of the beams and the decking in the vertical direction. Even if in a real building the decking would be fixed to the beams, thus enhancing the composite interaction and the overall stiffness, the floor would also be much thicker and heavier, due to the finishing. The structural assembly is not intended to be representative of realistic situations, it is a structural archetype useful for the accurate calibration of numerical models able to predict its vibration performance.

A slight and random brushing of the structures using a wooden stick represented the excitation source. This method aims to improve the signal-to-noise ratio of the measurements (Brincker and Ventura 2015). The Enhanced Frequency Domain Decomposition method (EFDD, (Brincker et al. 2001)) and the Stochastic Subspace Identification method (SSI-cov (Peeters and De Roeck 1999), SSI-dat (Van Overschee and De Moor 2012)), implemented by the authors in Python programming language, yielded the modal parameters from the acquired data for the wooden beams and decking under investigation. The EFDD method, which is a so-called non-parametric, frequency domain procedure, and SSI, which is a parametric, time-domain procedure, are probably among the two most used techniques for OMA.

The numerical characterisation of the dynamic response originated from Finite Element Modelling using the software SAP2000 (CSI 2020). The authors developed a set of models for each sub-assembly (i.e. beams and board) before the testing using standardised values for the material properties (i.e. from material standard and DoP). These models provided an expected response, which was useful to derive a proper setup and instrumentation plan. Two models reproduced the dynamics of the beams. The former derived from the one-dimensional "Frame elements" based on the Timoshenko beam theory, the latter originated from the use of "Solid elements", which are eight-node elements for modelling three-dimensional structures. The material property was defined as orthotropic to model the glulam. Thin "Shell elements" modelled the decking, with the plywood of the boards idealised as an orthotropic material. Unfortunately, SAP2000 does not perform a modal analysis of unrestrained objects. Therefore, a "Linear-link" element connected the modelled structures' end corners to the ground. An infinitesimal stiffness was assigned to the link elements to simulate the unrestrained boundary conditions.

The global model of the floor emerged from the sensitivity analysis and model updating of the structural sub-assemblies, see Fig3. "Linear-link" elements connect the beam's nodes to the nodes of the plywood boards. Each element is assumed to be composed of six separate "springs", each associated with a deformational degree of freedom (DoF). Given the type and source of loading, the authors assigned an infinite stiffness to the first local axis of the spring, representing the contact between components (see Fig3).Conversely, the other DoF were kept unrestrained since the boards were not fixed to the beams. The mesh size of the frame elements (50 mm), the solid elements (55x25x30 mm) and the shell elements (50x50 mm) derived from a simple convergence test on the firsts natural frequencies, and represent a possibly satisfactory compromise between accuracy and computational time.

The SAP2000 Open Application Programming Interface (OAPI) was used in combination with the open-source programming language Python to develop the routines for the sensitivity analysis and model updating. The OAPI allows third-party products, like Python, to interact with SAP2000, allowing the users to create custom applications.

A Sobol sensitivity analysis (Sobol 1993) evidenced the role of each term of the flexibility matrix of an orthotropic finite element. Namely, the analysis returned the sensitivity indices of the three MoE, E_X E_Y E_Z, the three Shear Moduli, G_{XY} G_{XZ} G_{YZ}, and three Poisson's ratios, ν_{YX} ν_{ZX} ν_{ZY} on the output (modal properties).

Finally, the FE models were tuned to reflect the measured data better using two global optimization algorithms for "black box" functions, the Differential Evolution (DE) (Storn and Price 1997) and the Particle Swarm Optimization (PSO)(Kennedy and Eberhart 1995). The script for the model updating process was written in Python using SAP2000 OAPI along with the Python module PySwarms (Miranda 2018) (to run PSO), and the popular Python toolkit SciPy (Virtanen et al. 2020)(to run DE). The idea behind PSO is to emulate the social behaviour of birds and fishes by initializing a set of candidate solutions to search for an optimum. A set of candidate solutions (called particles) are moved around in the search-space. The movements of the particles are guided by their own best-known position in the search-space as well as the entire swarm's best-known position. Differential evolution is a stochastic population-based method that, at each step, mutates each candidate solution (called agents) by mixing with other candidate solutions to create a trial candidate. If the new position is an improvement, then it is accepted and forms part of the population. Otherwise, the new position is simply discarded.

The following objective function measures the distance between the estimated modal parameters and the numerical ones:

$$C = \sum_{i=1}^{M} \gamma_i \left(\frac{f_i^m - f_i^c}{f_i^m} \right)^2 + \sum_{i=1}^{M} \beta_i \left(1 - MAC(\{\phi^m\}_i, \{\phi^c\}_i)\right) \tag{1}$$

where the apex $(*)^m$ indicates a measured variable, the apex $(*)^c$ a calculated variable, f_i is the i^{th} natural frequency, ϕ_i is the mode shape vector, M is the number of modes, MAC is the Modal Assurance Criterion, while γ_i and β_i are weighting factors.

Practitioners usually rely on simplified equation provided by building codes and standards to design structural elements, rather than rely on cumbersome and time-consuming FE analysis, especially at early design stages. To reflect this aspect the authors drew some comparisons to well-known engineering procedures. The bending vibrations of a beam can be described by the well-known Euler-Bernoulli beam equation:

$$EI \frac{\partial^4 z}{\partial x^4} + \rho A \frac{\partial^2 z}{\partial t^2} = 0 \quad with \quad 0 < x < L \tag{2}$$

where the E is the MoE, I is the second moment of inertia of the cross-section, ρ is the mass density (mass per unith length), A is the cross-section area, z is the vertical displacement, L is the length of the beam and t is time. The solution for Eq.(2) can be found for example by decomposing the displacement into a sum of harmonic vibrations $z(x,t) = Re[\hat{z}(x)e^{-i\omega t}]$. Eq.(2) can then be rewritten as an ordinary differential equation $EI\partial^4\hat{z}/\partial x^4 - \rho\omega^2\hat{z} = 0$, which have a general solution of the form:

$$\hat{z}_n = C_1 cosh(k_n x) + C_2 sinh(k_n x) + C_3 cos(k_n x) + C_4 sin(k_n x) \quad with \quad k_n = \left(\frac{\rho \omega_n^2}{EI} \right)^{1/4} \tag{3}$$

where $C_1 - C_4$ are constants that depend on the boundary conditions, k_n is the wave number and ω_n is the n^{th} natural frequency. Eurocode 5 (EN1995 2004) provides a formula to estimate the first natural frequency of rectangular floor with span L, width B, simply supported along the four edges, which derives from the temporal component of the solution of Eq.(3):

$$f_1 = \frac{\pi}{2L^2}\sqrt{\frac{(EI)_L}{m}} \tag{4}$$

where $(EI)_L$ is the equivalent bending stiffness along the span direction and m is the mass per unit floor area.

To sum-up the following steps were pursued after the dynamic testing of the elements:

- Sobol sensitivity analysis to find the most important mechanical parameters.
- Model updating to tune the numerical model to the experimental results.
- Comparison between experimental results, numerical model results and analytical model results.

DYNAMIC IDENTIFICATION

Experimental setup

The measurement chain was composed of ten seismic ceramic shear piezoelectric accelerometers, an HBM QuantumX data acquisition unit (24-bit analogue-to-digital converter) and a laptop pc. Shielded polyurethane coaxial cables made the connection between the sensors and the acquisition unit. The accelerometers (PCB, model 393B12) have an approximate 10000 mV/g sensitivity, a frequency range from 0.15 Hz to 1000 Hz and a measurement range up to $\approx \pm 5\ m/s^2$.

The accelerometers measured the beam responses parallel to the principal axes of inertia (strong and weak) in the free-free condition, according to the setups shown in Fig4a. Mounting studs and small metal plates screwed to the beams extrados (i.e. top surface) secured the accelerometers to the elements. The second setup for the weak axis allowed the extraction of the torsional modes of the beams, see Fig4c. In this case, three different measurements were processed and then merged to get the mode shapes. The sensors were attached to the beams through adhesive rubber to fasten up the testing operations. Furthermore, the beams were also tested on two metal supports to simulate the simply-supported condition; this time, the measurement axes were parallel to the strong axis of inertia. Fig4b shows the test setup of the decking. The authors tested a single panel out of the three plywood sheets. The testing of the structural sub-assembly had the sensors placed by the intrados of the beams. This choice allowed to leave the space on top of the floor free, see Fig2b. The accelerometers were evenly distributed along both beams. The distance between the edge accelerometers was lesser than the beam length due to the presence of the supports.

The sampling frequency was set to 1200 Hz (the aliasing filter is automatically set by the software embedded in the logger), and the duration was 5 minutes for every test. The data were first detrended to remove the DC offset with the application of a digital high-pass filter, then decimated. Different decimation factors, depending on the frequency bandwidth of interest, were used.

With regards to the EFDD method, the Power Spectral Densities (PSD) were estimated according to the Welch's method, dividing the data so as to get a frequency resolution of 0.1 Hz and using a Hanning window with 50% overlap. The MAC rejection level to estimate the singe-DoF PSD "bell" function was set to 0.95. Twenty consecutive peaks were used to estimate the damped frequency and the damping ratio from the autocorrelation function, ignoring the first 3. For the SSI-cov method, the number of block rows was set to 15, and the maximum model order to 80. As suggested in (Rainieri and Fabbrocino 2014), the stability requirements were set to:

$$\left(\frac{|f(n) - f(n+1)|}{f(n)}\right) < 0.01, \tag{5}$$

$$\left(\frac{|\xi(n) - \xi(n+1)|}{\xi(n)}\right) < 0.05, \tag{6}$$

$$[1 - MAC(\{\phi(n)\}, \{\phi(n+1)\})] < 0.02, \tag{7}$$

where (n) and $(n+1)$ are the n^{th} and $n^{th}+1$ model order, f is the natural frequency, ξ is the damping, and ϕ is the mode shape vector.

Results and discussion

Processing the data yielded nine of the first ten modes of the freely suspended beams in the bandwidth between 0 Hz and 300 Hz, the only exclusion being the first flexural mode along the weak axis. Tab1 shows the results estimated from the EFDD method and SSI-cov, with the results of the preliminary numerical model. As can be seen from the table, the estimated frequencies are very close to each other. The mode shape estimates are very consistent, with CrossMAC values higher than 0.99. Furthermore, the experimental results do not differ too much from the numerical ones. The only exception being the swapping of position between the 1^{st} flexural mode along the strong axis and the 2^{nd} flexural mode along the weak axis in the measured modes, compared to the numerical ones. Fig5 shows the experimental modes: the MAC matrix in Fig6 remarks on the excellent correspondence between experimental and numerical modes. The fact that some off-diagonal terms have very high values could seem odd at first glance, but with a more careful look, one can notice how these are the modes that have similar shape along the two orthogonal axes.

Three modes were identified in the bandwidth between 0 Hz and 300 Hz when the two beams were simply supported. Tab2 presents the results of dynamic identification compared to the results of the numerical model and the first three frequency calculated according to Eq.(3). The excellent crossMACs between analytical and numerical mode shapes confirm that the beam's meshing size for the numerical model was appropriately chosen.The experimental mode shapes are depicted in Fig7. A more significant difference between measured and numerical/analytical results is appreciable for the II and the III mode, both in terms of natural frequencies and mode shapes. The differences are probably due to the stiffness of the metal supports, which are not able to restrain the uplift movement.

Interestingly, the measured mode shapes, depicted in Fig7, reveal the presence of defects on both beams, which were not detectable when the beam was tested as freely suspended. The visible variations recorded by the accelerometers nearby the location of the damages, especially in the III mode, suggest that higher modes can be used as indicators to localise the presence of damages on structural elements, as already suggested by other authors (Ciambella et al. 2019; Aloisio et al. 2020e).

The identification of the plywood boards in Tab3 returned seven stable modes in the bandwidth $0 - 100\ Hz$. The numerical model evidenced the presence of some modes, not reported here, that could not be identified from the chosen setup. These are those modes where all the positions of the accelerometers correspond to the nodes of the mode shapes (i.e. a point of dynamic equilibrium), and therefore could not be detected. Out of the seven modes, three show a notable agreement with the numerical model, namely: mode I, mode VI and mode VII (see Fig8). The others seem to be more affected by the presence of the Rockwool pad. Looking more carefully at the mode shapes in Fig8 one can notice how in mode I, VI and VII, the central point is a node of the modal shape and accordingly less affected by the presence of the Rockwool. Whereas modes IV and V, where the centre is an anti-node, are more affected by the insulation piece.Nevertheless, the addition of a small set of springs at the centre of the numerical model, so as to simulate the presence of the Rockwool, determine mode IV and mode V to exhibit a satisfactory agreement with the experimental data, as remarked in the following paragraphs.

The dynamic identification of the simply-supported floor assembly returned two stable modes in the bandwidth $0 - 40\ Hz$, that is the suggested bandwidth of interest for timber floors (EN1995 2004). Mode I is a torsional mode were the two beams move out of phase with each other, while mode II is the first bending mode, namely the two beams are in phase. Tab4 reports the estimated frequencies and damping ratios with the results of the numerical model. The particular configuration of the floor, with the board not rigidly fixed to the beams, prompted the numerical model to exhibit several local modes of the boards that had almost no effect on the beams. The mode shapes from the numerical model were extracted from the modal displacement of nodes belonging to the frame elements, in order to be faithful to the test setup. The results of the two methods are in excellent agreement, with CrossMAC values higher than 0.99. In a single instance, the damping ratio of the II mode from SSIcov was noticeably higher than that estimated from the EFDD. The adoption of standardized material properties in the numerical model causes a significant error in terms of frequency, although the mode shapes show a satisfactory correspondence with the experimental. Moreover, in Tab4 the first bending frequency (mode II) can also be compared to the first bending frequency calculated according to the analytical Euler-Bernoulli model. The two frequency values reported correspond to the situation when a complete composite action between the beams and the decking and only the beams are respectively considered for the calculation of $(EI)_L$, in Eq.(4).

It is worthwhile to point out that exciting the tested structure did undoubtedly help to increase the signal to noise ratio, but it also partially masked the presence of spurious harmonics. Structures under test may show dominant frequency components which do not represent natural frequencies but derive from deterministic signals superimposed to the stochastic response (e.g., rotating equipment). One of the criteria to identify the presence of such spurious harmonics is by looking at the plot of the singular values of the PSD matrix. The PSD matrix presents a high rank in similar instances, and the spurious frequency is recognizable in the plot of the singular values, which have a sharp-pointed resonance peak. During the excitation, the peaks in the plot of the singular values could be misunderstood for natural frequencies. In the current case, a few tests carried out without the manual excitation revealed the occurrence of the spurious harmonics. Fig9 demonstrates this aspect by comparing the plots of the singular values of the floor assembly.

SENSITIVITY ANALYSIS AND MODEL UPDATING

Sensitivity analysis

The solid element models of the beams were the base of a variance-based sensitivity analysis. The analysis allowed decomposing the variance of the output (objective function, and natural frequencies) of the model into fractions which can be attributed to the inputs (mechanical properties). The first step was setting the inputs sampling range (mean value ±30%) and generate the model inputs according to the Saltelli's sampling scheme (Saisana et al. 2005) ($N * (2D + 2)$ model inputs were generated, where $N = 100$ is the number of samples, and $D = 9$ is the number of input parameters). After running all the model inputs the first-order (S1) and total-order (ST) sensitivity indices were calculated. S1 and ST measure respectively, the effect of varying a single parameter alone and the contribution to the output variance of the selected parameter including all variance caused by its interactions with the other parameters. Since the results were similar for both beams, Tab5 and Tab6 details those of a single beam. The first two columns express the impact of the mechanical parameters on the total response (Obj. Fun. = Objective Function). The following columns show the impact of the parameters on each mode (SA=Strong axis, WA=Weak axis, Tors=Torsional mode).

From Tab5 and Tab6 it is evident that the dynamic behaviour is mainly influenced by E_X and G_{XZ}, while G_{XY} shows a moderate contribution. The other parameters do not affect the results at all. For the objective function the differences in the first and total order indexes show some degree of interaction between E_X and G_{XZ}. Furthermore, between all the flexural modes, E_X is the most critical parameter. However, in the dynamic parallel to the strong axis, the shear modulus G_{XZ} gain importance in higher modes (see SAIII in Tab5). The fact that G_{XY} show very little influence for the modes along the weak axis agrees with the fact that the cross-section is much higher than wider (115 x 315 mm). This aspect is also evident in the torsional modes, where G_{XZ} is the most crucial parameter. These observations are in line with what one could expect from the slender nature of the element, which should indeed follow the assumptions of the beam theory.

The fact that some first-order indices add up to values slightly higher than one may derive from the reduced number of samples ($N = 100$). Still, this does not affect the substantial interpretation of the results. A 2^{nd} order polynomial was fitted to the values of the objective function to provide a graphical description of the results in the E_X and G_{XZ} domain, see Fig10.

Model Updating

Finite element model updating methods aim at tuning a numerical model to the measured response(Marwala 2010). It is assumed that the measurements are correct, and the model under consideration will need to be updated to reflect the measured data better.

As already mentioned, two global optimization algorithms headed the model updating process: particle swarm optimization (PSO) and differential evolution (DE). Eq.(1) was used in both to minimize the distance between measurements and numerical simulations. The results of the sensitivity analysis supported the adoption of β equal to 0.1. The choice counterbalanced the significant contribution of the second part of the objective function (due to the MAC). The swapping of position between the 1^{st} flexural mode along the strong axis and the 2^{nd} flexural mode along the weak axis resulted, in fact, in very high values of the objective function, see Fig10.

The natural frequencies depend on the ratio between the stiffness and the mass of the system. The direct weighting of the beams and the panel allowed a straightforward calibration of the FE model inertia (Beam 1 = $455 kg/m^3$, Beam 2 = $470 kg/m^3$, panel = $680 kg/m^3$). Tab7, Tab8 and Tab9, Tab10 report the frequencies of the initial FE models (with the measured mass), with errors to test results, referred to the frame and solid element models, respectively. The first update regarded the frame element. Isotropic material properties are used for these elements by SAP2000 even if the material is defined as orthotropic. However, the definition of the material as orthotropic allows to separately define the elastic modulus E_X (axial stiffness and bending stiffness) and the shear modulus G_{XZ} (transverse shear stiffness), which were the selected parameters to be updated in this model. The last columns of Tab7 and Tab8 list the frequencies of the updated FE model, compared to test results. The averages of the optimal solutions of the two algorithms, used to calculate the modes of the updated model, are presented in the lower part of Tab7 and Tab8. The tables reveal that the updating process did improve the agreement between the physical and numerical model. However, the model did not resolve the already mentioned inconsistency due to the swapping of position between modes. Furthermore, the updating of Beam 1 showed that there is a reduction of the elastic modulus E_X compared to the mean value of the standards, while that of Beam 2 E_X increases slightly. Likely, the reduction of the elastic modulus E_X in Beam 1 derives from the wide crack present by the end of the beam. The shear modulus G_{XZ} is higher than expected in both beams, more evident in Beam 2 than Beam 1.

In the second step, the updating regarded the solid beam models. Following the results of the sensitivity analysis, only E_X, G_{XZ} and G_{XY} were updated among the nine mechanical properties. The updating process involved G_{XY}, although the sensitivity analysis showed that this parameter has minimal effect on the dynamic behaviour in the selected frequency range. Similarly to the frame element model, Tab9 and Tab10 reports the results of the solid beam models. The last columns show the frequencies and the error of the updated model, while the lower part of the table reports the averages of the optimal solutions found by the two algorithms. This model yielded a significant improvement in the results. Still, as occurred in the frame-like models, the updating did not resolve the inconsistency due to the swapping of position between modes. There is a similar reduction of the elastic modulus E_X in Beam 1, probably caused by the cracks. Similar observations about the frame element model are valid about the shear modulus G_{XZ} of both beams. The shear modulus G_{XY} exhibits an increment to values suggested by the standards in the Beam 2. In contrast, there is a decrease in the shear modulus G_{XY} in Beam 1. The results in terms of MAC are very high (≈ 0.99), except for the inconsistency between the first modes.

The sensitivity analysis and the model updating process confirm that the "solid elements" model does not determine a significant enhancement of the results to the "frame elements" model. For these reasons, the use of "solid elements" for the FE model of the floor assembly is worthless, given the enormous computational costs related to the use of the "solid elements" model.

The use of low-stiffness linear links (100 N/mm) placed by the middle of the plate, in correspondence of the Rockwool pad, enhance the quality of the results referred to mode IV and V. The first column of Tab3 and the second column of Tab11 prove this aspect. Conversely, the low-stiffness linear links did not affect the results of mode I, VI and VII: the centre is a node in these modes. Accordingly, the authors used only mode I, VI and VII to update the FE model with the optimization algorithms as carried out in the beam models. The last columns of Tab11 summarize the results, while the lower part of the table reports the optimal solutions (rounded).

The numerical model of the floor assembly was built after the updating of the single structural components. As already mentioned, frame elements were used to model the beams and shell elements the plywood boards. The boards were "lifted" to the centre of mass of the beams. Link elements, with infinite stiffness in the axial direction and zero stiffness to all the others, model the connection between the elements. The updated parameters of the single sub-assemblies yield already a good match with the measurements (compare the first columns of Tab12). However, it was decided to enhance it further, by changing the supports' stiffness from infinite into a finite value. The simplicity of the problem encouraged a manual update based on trial and error. Tab12lists the results of the updated FE model with the optimal solution. As further validation, the estimated stiffness value of the supports was applied to the simply-supported beam models. The adoption of a finite value of stiffness of the supports determine a further enhancement of the results, see Tab13. It was observed that a higher stiffness for the supports was needed to reduce the frequency discrepancy further.

The findings of the investigation confirm that the dynamic response of a timber floor is highly sensitive to every parameter that describe its components and its boundary conditions. Unfortunately predicting accurately the dynamical behaviour of a timber floor with simplified analytical approach is rarely possible. Even if well-known and understood analytical models are certainly useful at preliminary design stages, more detailed numerical models are needed if high level of performance of the floor are desired. It is possible to obtain numerical models very faithful to reality, however updating every element that composes the system is not feasible in practical applications. To assess the behaviour of an existing floor in a building, a researcher would need update all the parameters "at once" with an inevitable loss of detail. A careful examination of the drawings corroborated by on-site inspections is therefore of paramount importance in order to build a detailed and representative numerical model. Furthermore the level of detail of the experimental campaign will set the basis for the success of the updating process.

CONCLUSIONS

This paper investigates the dynamic behaviour of a simply-supported timber floor assembly and its composing elements. A sensitivity analysis revealed the influence of mechanical parameters on the dynamic response. As the last step, the numerical models were updated to reflect the findings of the measurements better. The main findings are:

- OMA techniques can be used, instead of EMA techniques, to test not only massive civil engineering structures, but also smaller structural elements, such as floors, beams etc., and their results can be used to calibrate the parameters of numerical models.

- It is helpful to continuously and randomly excite the tested components, for example, by rubbing something onto it, to increase the signal-to-noise ratio. Significant attention must, however, be paid not to mistake spurious harmonics for natural frequencies.
- Small pieces/layers of insulation material, can be used to recreate free-free boundary conditions if the suspension of the element is not possible.
- Higher modes were found more susceptible to damages and defect when the beams were tested as simply-supported. They could therefore be used as damage indicators to assess the state of health and/or to localise defects in it. When the beams were tested as freely suspended, however, the damages seemed not to affect the modal shapes.
- The results of the identification, for any component, are very susceptible to the nature of the boundary conditions and even small variations in them significantly affect the results.
- The results confirm that the use of the well-known beam model is more than capable of correctly predicting the behaviour of slender components. The significant computational time needed for a solid element model is not worth the gain in terms of precision.

This research was preliminary to more-in-depth investigations about the walked-induced vibration response of timber floors. The authors aim at using the assembled floor system and the updated numerical model to study different walking models further and compare numerical simulations with walking tests. This investigation will allow studying the various metrics used by building codes and relevant standards to evaluate and assess building floor vibrations.

DATA AVAILABILITY STATEMENT

Some or all data, models, or code that support the findings of this study are available from the corresponding author upon reasonable request.

ACKNOWLEDGEMENTS

The authors acknowledge the significant role of Prof. Rocco Alaggio, who shared with the authors his thirty years experience in dynamic identification.

REFERENCES

Aloisio, A., Alaggio, R., and Fragiacomo, M. (2020a). "Dynamic identification and model updating of full-scale concrete box girders based on the experimental torsional response." *Construction and Building Materials*.

Aloisio, A., Alaggio, R., and Fragiacomo, M. (2020b). "Fragility functions and behavior factors estimation of multi-story cross-laminated timber structures characterized by an energy-dependent hysteretic model." *Earthquake Spectra*, 8755293020936696.

Aloisio, A., Alaggio, R., and Fragiacomo, M. (2020c). "Time-domain identification of elastic modulus of simply supported box girders under moving loads: method and full-scale validation." *Engineering Structures*.

Aloisio, A., Alaggio, R., and Fragiacomo, M. (2021). "Equivalent viscous damping of cross-laminated timber structural archetypes." *Journal of Structural Engineering*, 147(4), 04021012.

Aloisio, A., Battista, L. D., Alaggio, R., Antonacci, E., and Fragiacomo, M. (2020d). "Assessment of structural interventions using bayesian updating and subspace-based fault detection methods: the case study of s. maria di collemaggio basilica, l'aquila, italy." *Structure and Infrastructure Engineering*, 1–15.

Aloisio, A., Di Battista, L., Alaggio, R., and Fragiacomo, M. (2020e). "Sensitivity analysis of subspace-based damage indicators under changes in ambient excitation covariance, severity and location of damage." *Engineering Structures*, 208, 110235.

Aloisio, A., Pasca, D., Tomasi, R., and Fragiacomo, M. (2020f). "Dynamic identification and model updating of an eight-storey clt building." *Engineering Structures*, 213, 110593.

Antonacci, E., Aloisio, A., Galeota, D., and Alaggio, R. (2020). "The s. maria di collemaggio basilica: From vulnerability assessment to first results of shm." *Journal of Architectural Engineering*, 26(3), 05020007.

Bedon, C. and Morassi, A. (2014). "Dynamic testing and parameter identification of a base-isolated bridge." *Engineering Structures*, 60, 85–99.

Brandner, R., Flatscher, G., Ringhofer, A., Schickhofer, G., and Thiel, A. (2016). "Cross laminated timber (clt): overview and development." *European Journal of Wood and Wood Products*, 74(3), 331–351.

Brincker, R. and Ventura, C. (2015). *Introduction to operational modal analysis*. John Wiley & Sons.

Brincker, R., Zhang, L., and Andersen, P. (2001). "Modal identification of output-only systems using frequency domain decomposition." *Smart materials and structures*, 10(3), 441.

Casagrande, D., Giongo, I., Pederzolli, F., Franciosi, A., and Piazza, M. (2018). "Analytical, numerical and experimental assessment of vibration performance in timber floors." *Engineering Structures*, 168, 748–758.

Ceccotti, A., Sandhaas, C., Okabe, M., Yasumura, M., Minowa, C., and Kawai, N. (2013). "Sofie project–3d shaking table test on a seven-storey full-scale cross-laminated timber building." *Earthquake Engineering & Structural Dynamics*, 42(13), 2003–2021.

Ciambella, J., Pau, A., and Vestroni, F. (2019). "Modal curvature-based damage localization in weakly damaged continuous beams." *Mechanical Systems and Signal Processing*, 121, 171–182.

CSI (2020). "Sap2000 v21. integrated software for structural analysis & design." *Computers and Structures, Inc., Berkeley, California, USA*.

Devriendt, C., Magalhães, F., Weijtjens, W., De Sitter, G., Cunha, Á., and Guillaume, P. (2014). "Structural health monitoring of offshore wind turbines using automated operational modal analysis." *Structural Health Monitoring*, 13(6), 644–659.

EN14080 - Timber structures. Glued laminated timber and glued solid timber. Requirements (2013). European Committee for Standardisation.

EN 1995-1-1: 2004—Eurocode 5: Design of timber structures—Part 1-1: General—Common rules and rules for buildings (2004). European Committee for Standardisation.

Friswell, M. and Mottershead, J. E. (2013). *Finite element model updating in structural dynamics*, Vol. 38. Springer Science & Business Media.

Gentile, C., Ruccolo, A., and Canali, F. (2019). "Long-term monitoring for the condition-based structural maintenance of the milan cathedral." *Construction and Building Materials*, 228, 117101.

Hamm, P., Richter, A., and Winter, S. (2010). "Floor vibrations–new results." *Proceedings of 11th World Conference on Timber Engineerig (WCTE2010), Riva del Garda*.

Hu, L. J., Chui, Y. H., and Onysko, D. M. (2001). "Vibration serviceability of timber floors in residential construction." *Progress in Structural Engineering and Materials*, 3(3), 228–237.

Huang, H., Gao, Y., and Chang, W.-S. (2020). "Human-induced vibration of cross-laminated timber (clt) floor under different boundary conditions." *Engineering Structures*, 204, 110016.

Izzi, M., Casagrande, D., Bezzi, S., Pasca, D., Follesa, M., and Tomasi, R. (2018). "Seismic behaviour of cross-laminated timber structures: A state-of-the-art review." *Engineering Structures*, 170, 42–52.

Kennedy, J. and Eberhart, R. (1995). "Particle swarm optimization." *Proceedings of ICNN'95-International Conference on Neural Networks*, Vol. 4, IEEE, 1942–1948.

Kita, A., Cavalagli, N., and Ubertini, F. (2019). "Temperature effects on static and dynamic behavior of consoli palace in gubbio, italy." *Mechanical Systems and Signal Processing*, 120, 180–202.

Magalhães, F., Caetano, E., and Cunha, Á. (2008). "Operational modal analysis and finite element model correlation of the braga stadium suspended roof." *Engineering Structures*, 30(6), 1688–1698.

Marwala, T. (2010). *Finite element model updating using computational intelligence techniques: applications to structural dynamics*. Springer Science & Business Media.

Miranda, L. J. V. (2018). "PySwarms, a research-toolkit for Particle Swarm Optimization in Python." *Journal of Open Source Software*, 3.

Mugabo, I., Barbosa, A. R., Riggio, M., and Batti, J. (2019). "Ambient vibration measurement data of a four-story mass timber building." *Frontiers in Built Environment*, 5, 67.

Ohlsson, S. V. (1982). *Floor vibrations and human discomfort*. Chalmers University of Technology, Division of Steel and Timber Structures.

Peeters, B. and De Roeck, G. (1999). "Reference-based stochastic subspace identification for output-only modal analysis." *Mechanical systems and signal processing*, 13(6), 855–878.

Peeters, B., Van der Auweraer, H., Vanhollebeke, F., and Guillaume, P. (2007). “Operational modal analysis for estimating the dynamic properties of a stadium structure during a football game.” *Shock and Vibration*, 14(4), 283–303.

Pereira, S., Magalhaes, F., Gomes, J. P., Cunha, A., and Lemos, J. V. (2018). “Dynamic monitoring of a concrete arch dam during the first filling of the reservoir.” *Engineering Structures*, 174, 548–560.

Rainieri, C. and Fabbrocino, G. (2014). “Operational modal analysis of civil engineering structures.” *Springer, New York*, 142, 143.

Rainieri, C., Magalhaes, F., Gargaro, D., Fabbrocino, G., and Cunha, A. (2019). “Predicting the variability of natural frequencies and its causes by second-order blind identification.” *Structural Health Monitoring*, 18(2), 486–507.

Reynders, E., Houbrechts, J., and De Roeck, G. (2012). “Fully automated (operational) modal analysis.” *Mechanical Systems and Signal Processing*, 29, 228–250.

Reynders, E., Maes, K., Lombaert, G., and De Roeck, G. (2016). “Uncertainty quantification in operational modal analysis with stochastic subspace identification: validation and applications.” *Mechanical Systems and Signal Processing*, 66, 13–30.

Reynolds, T., Casagrande, D., and Tomasi, R. (2016). “Comparison of multi-storey cross-laminated timber and timber frame buildings by in situ modal analysis.” *Construction and Building Materials*, 102, 1009–1017.

Saisana, M., Saltelli, A., and Tarantola, S. (2005). “Uncertainty and sensitivity analysis techniques as tools for the quality assessment of composite indicators.” *Journal of the Royal Statistical Society: Series A (Statistics in Society)*, 168(2), 307–323.

Sevim, B., Bayraktar, A., and Altunişik, A. C. (2011). “Finite element model calibration of berke arch dam using operational modal testing.” *Journal of vibration and control*, 17(7), 1065–1079.

Smith, A. L., Hicks, S. J., and Devine, P. J. (2007). *Design of floors for vibration: A new approach*. Steel Construction Institute Ascot, Berkshire, UK.

Smith, I. and Chui, Y. H. (1988). “Design of lightweight wooden floors to avoid human discomfort.”

Canadian Journal of Civil Engineering, 15(2), 254–262.

Sobol, I. M. (1993). “Sensitivity estimates for nonlinear mathematical models.” *Mathematical modelling and computational experiments*, 1(4), 407–414.

Storn, R. and Price, K. (1997). “Differential evolution–a simple and efficient heuristic for global optimization over continuous spaces.” *Journal of global optimization*, 11(4), 341–359.

Tcherniak, D., Chauhan, S., and Hansen, M. H. (2011). “Applicability limits of operational modal analysis to operational wind turbines.” *Structural Dynamics and Renewable Energy, Volume 1*, Springer, 317–327.

Van Overschee, P. and De Moor, B. (2012). *Subspace identification for linear systems: Theory—Implementation—Applications*. Springer Science & Business Media.

Virtanen, P., Gommers, R., Oliphant, T. E., Haberland, M., Reddy, T., Cournapeau, D., Burovski, E., Peterson, P., Weckesser, W., Bright, J., van der Walt, S. J., Brett, M., Wilson, J., Jarrod Millman, K., Mayorov, N., Nelson, A. R. J., Jones, E., Kern, R., Larson, E., Carey, C., Polat, İ., Feng, Y., Moore, E. W., Vand erPlas, J., Laxalde, D., Perktold, J., Cimrman, R., Henriksen, I., Quintero, E. A., Harris, C. R., Archibald, A. M., Ribeiro, A. H., Pedregosa, F., van Mulbregt, P., and Contributors, S. . . (2020). “SciPy 1.0: Fundamental Algorithms for Scientific Computing in Python.” *Nature Methods*, 17, 261–272.

Weckendorf, J., Hafeez, G., Doudak, G., and Smith, I. (2014). “Floor vibration serviceability problems in wood light-frame buildings.” *Journal of Performance of Constructed Facilities*, 28(6), A4014003.

Weckendorf, J. and Smith, I. (2012). “Dynamic characteristics of shallow floors with cross-laminated-timber spines.” *World*, 15, 19.

Weckendorf, J., Ussher, E., and Smith, I. (2016). “Dynamic response of clt plate systems in the context of timber and hybrid construction.” *Composite Structures*, 157, 412–423.

Xie, Z., Hu, X., Du, H., and Zhang, X. (2020). “Vibration behavior of timber-concrete composite floor under human-induced excitation.” *Journal of Building Engineering*, 101744.

List of Tables

TABLE 1. Results dynamic identification freely suspended beams

	SAP2000	Beam 1 SSIcov		Beam 1 EFDD		Beam 2 SSIcov		Beam 2 EFDD	
Mode	f_n[Hz]	f_n[Hz]	ξ[%]	f_n[Hz]	ξ[%]	f_n[Hz]	ξ[%]	f_n[Hz]	ξ[%]
1-Flex-WA	25.81	-	-	-	-	-	-	-	-
2-Flex-WA	69.96	62.98	0.72%	63.06	0.59%	65.66	0.61%	65.83	0.60%
1-Flex-SA	67.57	65.50	1.03%	65.98	1.00%	67.77	0.89%	67.54	1.13%
1-Tors	72.78	70.32	1.05%	70.52	1.07%	71.94	1.28%	71.51	0.85%
3-Flex-WA	133.75	124.09	0.99%	124.87	1.01%	129.50	0.89%	129.42	0.92%
2-Tors	146.86	149.15	2.12%	148.99	1.61%	154.37	2.24%	153.44	1.96%
2-Flex-SA	166.79	154.07	0.59%	155.97	0.54%	157.90	0.70%	157.91	0.66%
4-Flex-WA	214.06	194.83	0.59%	195.13	0.53%	202.75	0.65%	202.03	0.65%
3-Tors	223.42	220.05	2.53%	219.88	1.60%	227.53	3.55%	222.68	1.49%
3-Flex-SA	286.77	273.90	0.80%	273.68	0.73%	279.31	0.83%	278.40	0.73%

Flex = Flexural mode; Tors = Torsional mode; WA = Weak Axis; SA = Strong Axis
Numerical and analytical model's parameters:
$E_x = 13000\ [MPa]$, $G_{xz} = G_{xy} = 650\ [MPa]$; $\rho = 430\ [kg/m^3]$

TABLE 2. Results dynamic identification simply supported beams

Mode	SAP2000	Analytical	Beam 1 - SSIcov		Beam2 - SSIcov	
	f_n[Hz]	f_n[Hz]	f_n[Hz]	ξ[%]	f_n[Hz]	ξ[%]
I	32.72	31.42	28.90	0.70%	29.93	0.75%
II	117.77	125.66	90.22	1.76%	92.53	2.04%
III	230.84	282.74	149.50	1.75%	153.73	1.80%

Numerical and analytical model's parameters:
$E_x = 13000\ [MPa]$; $G_{xz} = G_{xy} = 650\ [MPa]$; $\rho = 430\ [kg/m^3]$;
$K_{support} = \infty$

TABLE 3. Results dynamic identification plywood boards

	SAP2000	Plate - SSIcov			Plate - EFDD		
Mode	f_n [Hz]	f_n [Hz]	ξ [%]	MAC	f_n [Hz]	ξ [%]	MAC
I	28.04	30.42	0.88%	95.8%	30.50	0.88%	96.0%
II	35.48	37.45	1.39%	51.2%	37.32	1.46%	51.6%
III	39.20	39.96	1.62%	47.8%	40.09	1.21%	48.8%
IV	35.36	46.90	2.80%	30.3%	47.05	1.63%	30.1%
V	61.90	74.29	5.86%	92.9%	74.45	5.24%	91.4%
VI	81.16	88.83	1.40%	98.6%	89.03	0.76%	98.9%
VII	93.56	91.24	1.58%	98.6%	91.08	0.74%	98.8%

Numerical model's parameters:
$E_x = 6000\ [MPa]$, $E_y = 8000\ [MPa]$; $\rho = 650\ [kg/m^3]$

TABLE 4. Results dynamic identification floor

	SAP2000	Analytical	Floor - SSIcov			Floor - EFDD		
Mode	f_n [Hz]	f_n [Hz]	f_n [Hz]	ξ [%]	MAC	f_n [Hz]	ξ [%]	MAC
I	20.09	-	16.76	3.26%	90.9%	16.81	3.28%	92.2%
II	23.44	26.37 / 23.41	20.28	3.96%	91.5%	20.31	2.40%	93.5%

Numerical model's parameters:
Glulam: $E_x = 13000$ $[MPa]$, $G_{xz} = 650$ $[MPa]$; $\rho = 430$ $[kg/m^3]$
Plywood: $E_x = 6000$ $[MPa]$, $E_y = 8000$ $[MPa]$; $\rho = 650$ $[kg/m^3]$
Supports: $K_{support} = \infty$

TABLE 5. First-order (S1) and total-order (ST) sensitivity indices for beam 1. Part I

	Obj. Fun.		SA I		SA II		SA III		WA II	
Param.	S1	ST	S1	ST	S1	ST	S1	ST	S1	ST
E_X	60%	80%	97%	97%	85%	86%	62%	64%	97%	97%
E_Y	0%	0%	0%	0%	0%	0%	0%	0%	0%	0%
E_Z	0%	0%	0%	0%	0%	0%	0%	0%	0%	0%
ν_{YX}	0%	0%	0%	0%	0%	0%	0%	0%	0%	0%
ν_{ZX}	0%	0%	0%	0%	0%	0%	0%	0%	0%	0%
ν_{YZ}	0%	0%	0%	0%	0%	0%	0%	0%	0%	0%
G_{XY}	0%	5%	0%	0%	0%	0%	0%	0%	0%	0%
G_{XZ}	32%	56%	1%	1%	10%	11%	32%	35%	0%	0%
G_{YZ}	0%	0%	0%	0%	0%	0%	0%	0%	0%	0%

TABLE 6. First-order (S1) and total-order (ST) sensitivity indices for beam 1. Part II

	WA III		WA IV		Tor I		Tor II		Tor III	
Param.	S1	ST	S1	ST	S1	ST	S1	ST	S1	ST
E_X	96%	96%	94%	94%	0%	0%	0%	0%	0%	1%
E_Y	0%	0%	0%	0%	0%	0%	0%	0%	0%	0%
E_Z	0%	0%	0%	0%	0%	0%	0%	0%	0%	0%
ν_{YX}	0%	0%	0%	0%	0%	0%	0%	0%	0%	0%
ν_{ZX}	0%	0%	0%	0%	0%	0%	0%	0%	0%	0%
ν_{YZ}	0%	0%	0%	0%	0%	0%	0%	0%	0%	0%
G_{XY}	1%	1%	3%	3%	3%	3%	4%	4%	5%	5%
G_{XZ}	0%	0%	0%	0%	101%	101%	100%	100%	98%	98%
G_{YZ}	0%	0%	0%	0%	0%	0%	0%	0%	0%	0%

TABLE 7. Result of the model updating on the "Frame elements" beam model. Beam 1

	Beam 1				
	Experimental	FE Initial model		Optimised model	
Mode	f_n[Hz]	f_n[Hz]	Error	f_n[Hz]	Error
1-Flex-SA	65.50	66.14	-0.97%	62.94	3.92%
2-Flex-WA	62.98	68.08	-8.09%	64.61	-2.59%
3-Flex-WA	124.09	129.17	-4.09%	123.76	0.26%
2-Flex-SA	154.07	163.31	-5.99%	157.12	-1.98%
4-Flex-WA	194.83	207.78	-6.65%	198.49	-1.88%
3-Flex-SA	273.90	280.09	-2.26%	272.34	0.57%
Optimal parameters:					
E_x = 11800 $[MPa]$; G_{xz} = 670 $[MPa]$; ρ = 455 $[kg/m^3]$					

TABLE 8. Result of the model updating on the "Frame elements" beam model. Beam 2

Beam 2					
	Experimental	FE Initial model		Optimised model	
Mode	f_n[Hz]	f_n[Hz]	Error	f_n[Hz]	Error
1-Flex-SA	67.77	65.21	3.77%	65.01	4.07%
2-Flex-WA	66.24	67.12	-1.33%	66.74	-0.76%
3-Flex-WA	129.86	128.19	1.28%	127.83	1.56%
2-Flex-SA	157.90	161.02	-1.98%	162.40	-2.85%
4-Flex-WA	202.75	204.87	-1.05%	205.07	-1.15%
3-Flex-SA	279.31	276.16	1.13%	281.68	-0.85%
Optimal parameters:					
$E_x = 13100\ [MPa]$; $G_{xz} = 700\ [MPa]$; $\rho = 467\ [kg/m^3]$					

TABLE 9. Results of the updating on the "Solid elements" beam model. Beam 1

	Beam 1				
	Experimental	FE Initial model		Optimised model	
Mode	f_n[Hz]	f_n[Hz]	Error	f_n[Hz]	Error
1-Flex-SA	65.50	65.76	-0.39%	62.54	4.52%
2-Flex-WA	62.50	68.08	-8.94%	64.35	-2.97%
1-Tors	70.32	70.83	-0.73%	72.15	-2.60%
3-Flex-WA	124.17	130.17	-4.83%	123.12	0.85%
2-Tors	149.15	142.92	4.17%	145.20	2.65%
2-Flex-SA	154.07	162.32	-5.35%	156.52	-1.59%
4-Flex-WA	193.55	208.32	-7.63%	197.20	-1.89%
3-Tors	220.05	217.43	1.19%	219.99	0.03%
3-Flex-SA	273.90	279.08	-1.89%	272.75	0.42%

Optimal parameters:
E_x = 11600 $[MPa]$; G_{xz} = 690 $[MPa]$; G_{xy} = 620 $[MPa]$;
ρ = 455 $[kg/m^3]$

TABLE 10. Results of the updating on the "Solid elements" beam model. Beam 2

	Beam 2				
	Experimental	FE Initial model		Optimised model	
Mode	f_n[Hz]	f_n[Hz]	Error	f_n[Hz]	Error
1-Flex-SA	67.77	64.84	4.32%	64.71	4.50%
2-Flex-WA	65.66	67.13	-2.24%	66.74	-1.65%
1-Tors	71.94	69.84	2.92%	74.15	-3.07%
3-Flex-WA	129.50	128.35	0.89%	127.86	1.26%
2-Tors	154.37	140.92	8.71%	149.27	3.30%
2-Flex-SA	157.90	160.05	-1.36%	161.62	-2.36%
4-Flex-WA	201.36	205.40	-2.01%	205.14	-1.87%
3-Tors	227.53	214.38	5.78%	226.28	0.55%
3-Flex-SA	279.31	275.17	1.48%	281.06	-0.63%
Optimal parameters: $E_x = 12800\ [MPa]$; $G_{xz} = 740\ [MPa]$; $G_{xy} = 700\ [MPa]$; $\rho = 467\ [kg/m^3]$					

TABLE 11. Results of the updating of the Plywood board

	Experimental	FE Initial model		Optimised model		
Mode	f_n[Hz]	f_n[Hz]	Error	f_n[Hz]	Error	MAC
I	30.42	28.31	6.9%	29.51	3.0%	99.8%
II	37.45	35.57	5.0%	37.60	-0.4%	47.8%
III	39.96	39.27	1.7%	38.87	2.7%	51.5%
IV	46.90	44.07	6.0%	44.66	4.8%	95.9%
V	74.29	71.02	4.4%	71.58	3.7%	98.9%
VI	88.83	81.39	8.4%	89.23	-0.5%	98.2%
VII	91.24	93.75	-2.8%	92.10	-0.9%	98.3%
Optimal parameters:						
$E_X = 6500\ [MPa]$; $E_Y = 7500\ [MPa]$; $\rho = 680\ [kg/m^3]$						

TABLE 12. Results of the updating of the floor

Mode	Experimental f_n [Hz]	FE Initial model f_n [Hz]	Error	Optimised model f_n [Hz]	Error	MAC
I	16.76	18.62	-11.11%	17.15	-2.32%	94.0%
II	20.30	21.77	-7.22%	20.30	0.00%	93.5%

Optimal parameters:
Glulam: see Tab6
Plywood: see Tab8
Supports: $K_{support}$ = 6000 $[N/mm]$

TABLE 13. Simply supported beam with updated parameters

	Experimental		FE Updated		FE Updated	
Mode	Beam 1	Beam 2	Beam 1	MAC	Beam 2	MAC
I	28.90	29.93	28.77	99.9%	29.74	100.0%
II	90.22	92.53	90.49	99.8%	92.17	99.5%
III	149.50	153.73	150.48	96.0%	151.67	92.5%

Optimal parameters:
Glulam: see Tab6
Supports: $K_{support}$ = 9000 $[N/mm]$

List of Figures

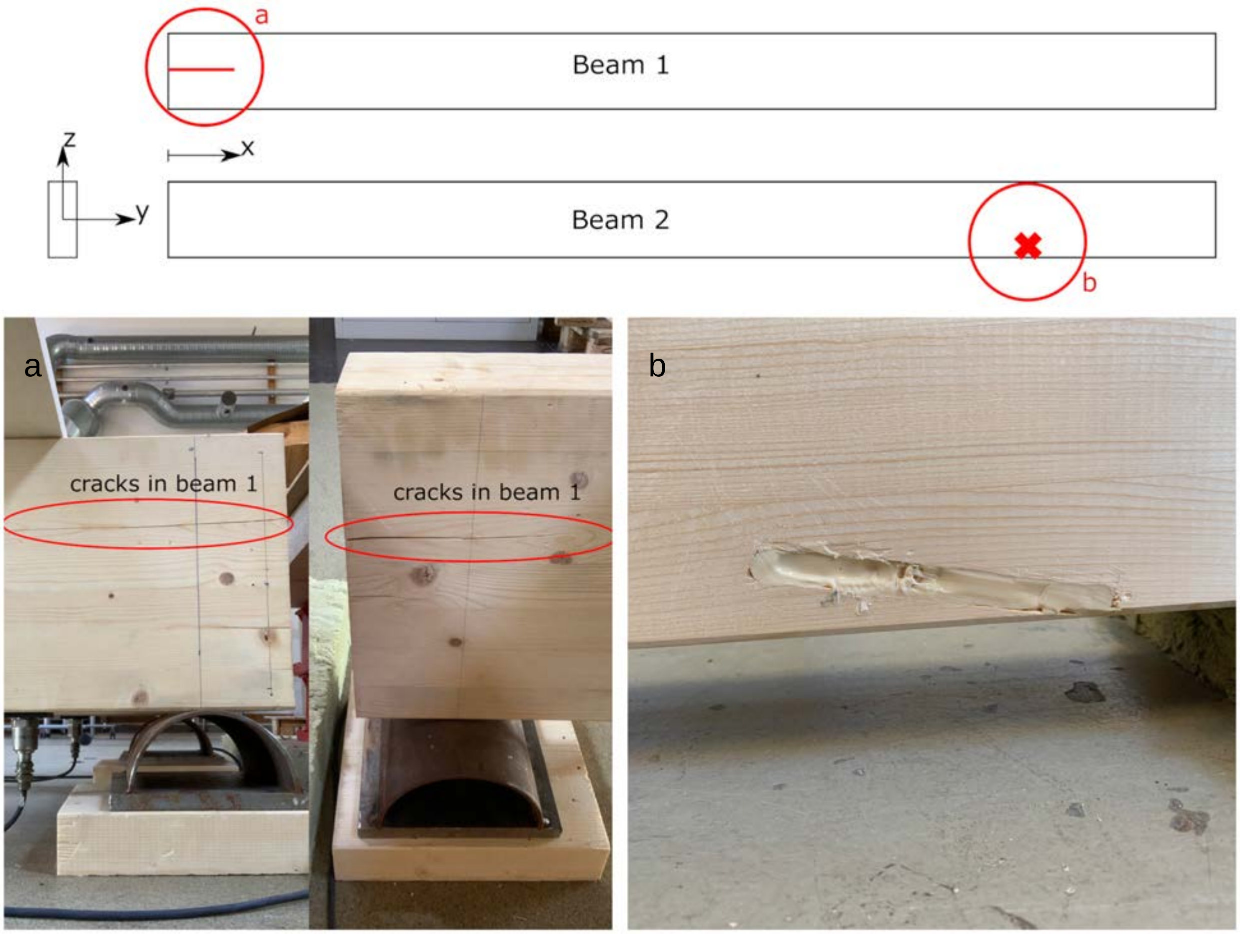

Fig. 1. Location of the defects on "Beam 1" and "Beam 2".

Fig. 2. Floor assembly: left view from above, right view from below.

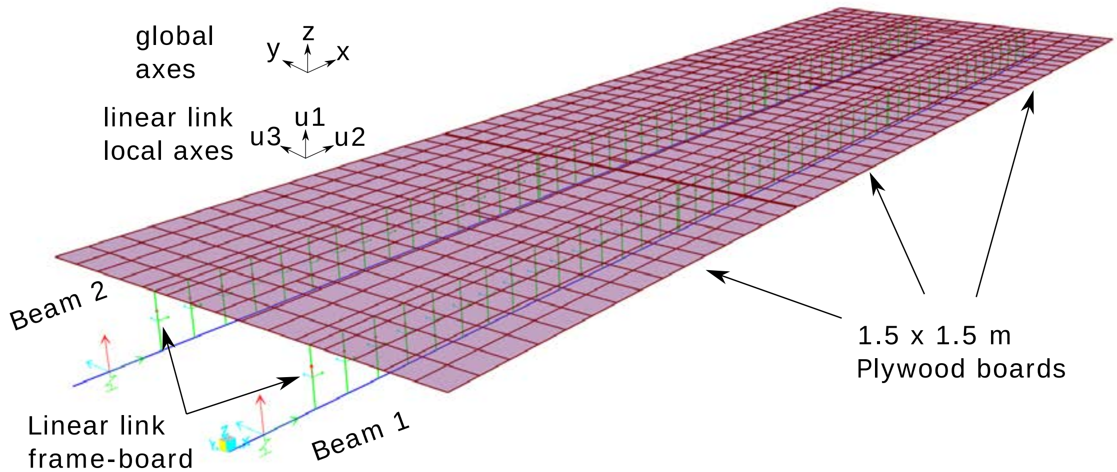

Fig. 3. Sap2000 FE model of the floor.

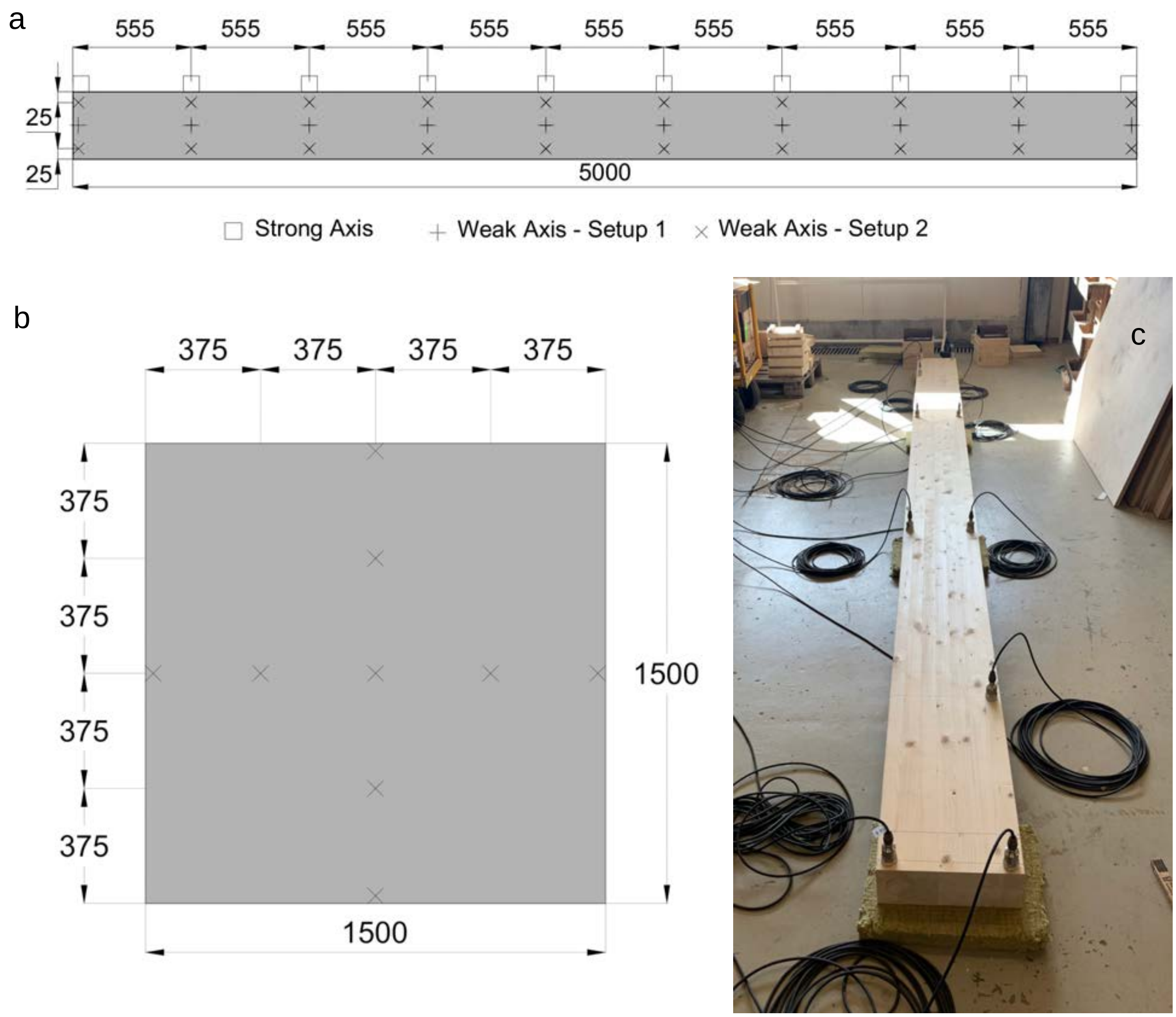

Fig. 4. a)Test setup glulam beams, b)Test setup plywood boards, c)Test setup for torsional modes glulam beams. (all the dimensions are in mm)

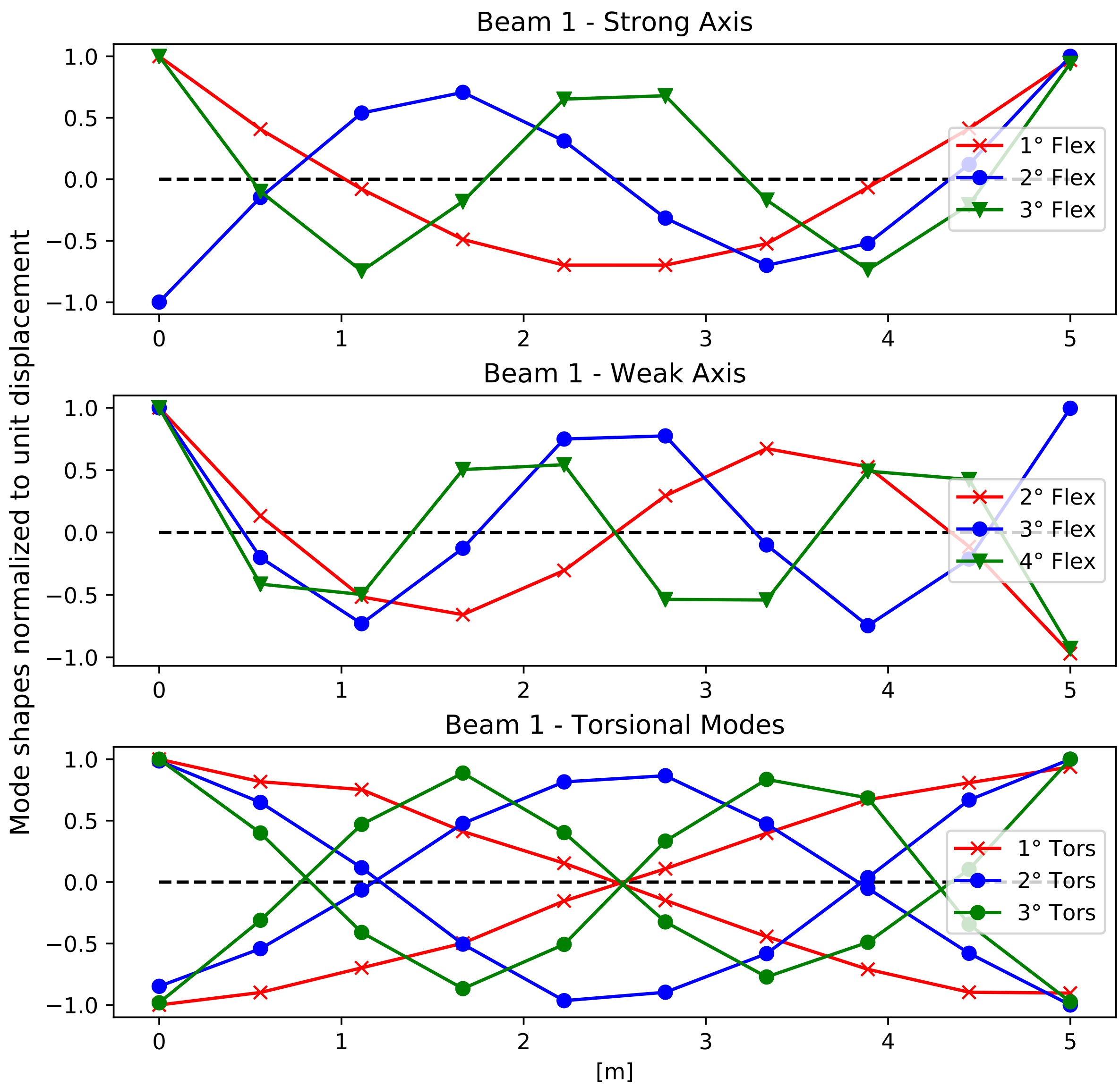

Fig. 5. Experimental modal shapes freely suspended beam.

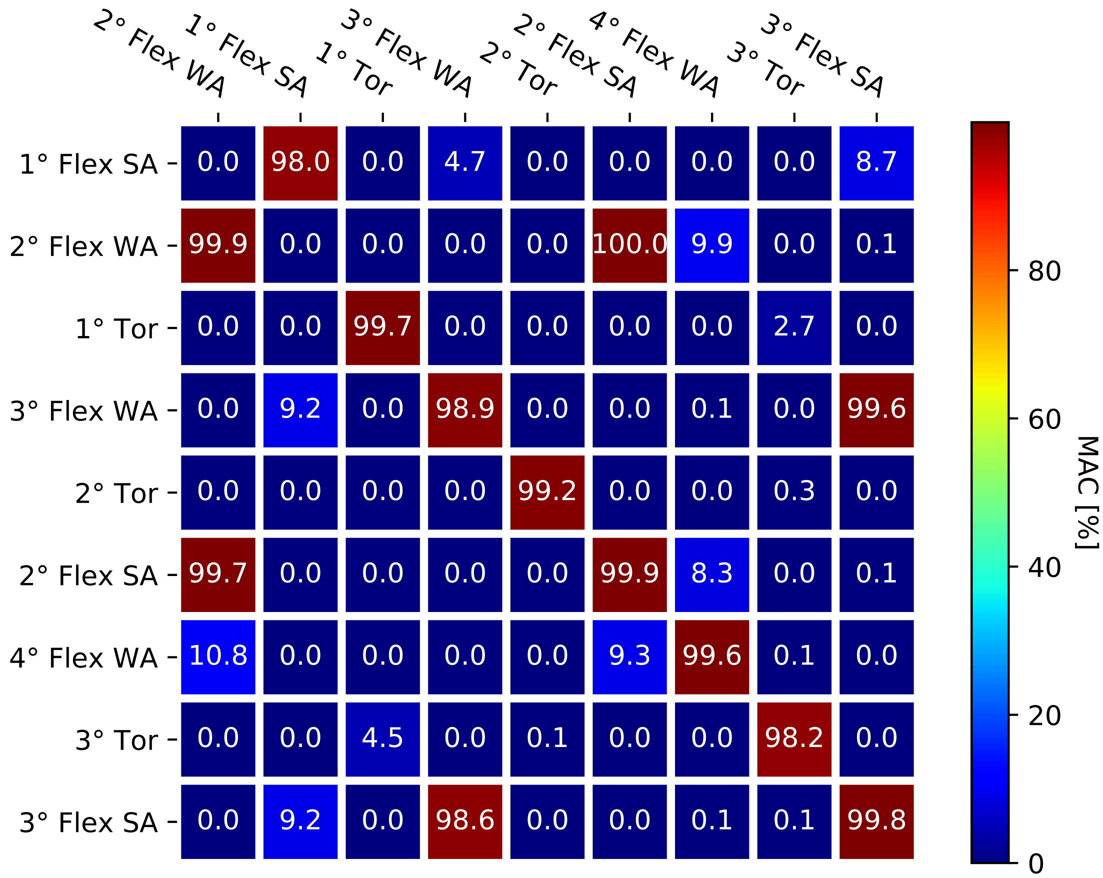

Fig. 6. MAC matrix: measured mode shapes vs numerical.

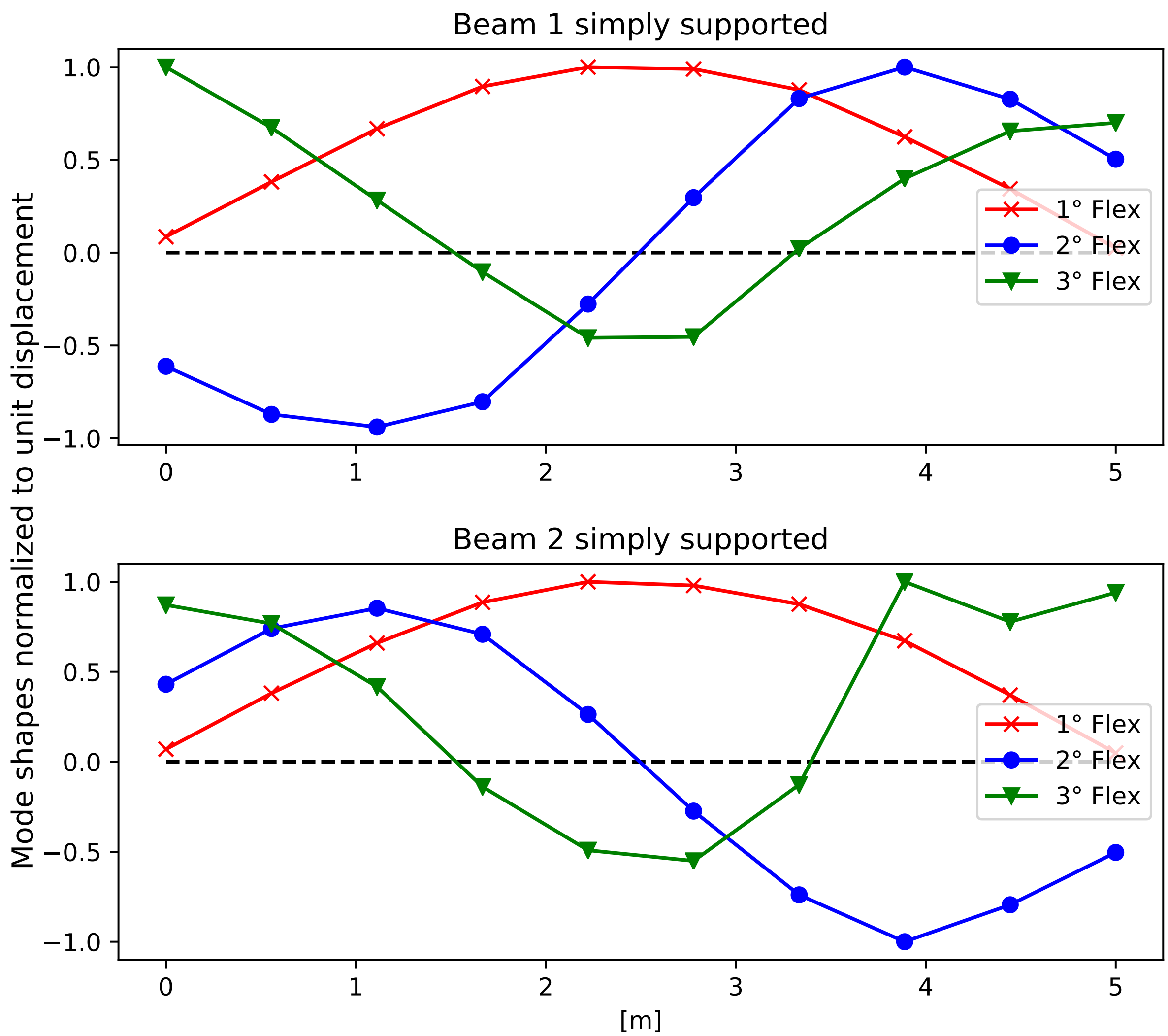

Fig. 7. Experimental modal shapes simply supported beam.

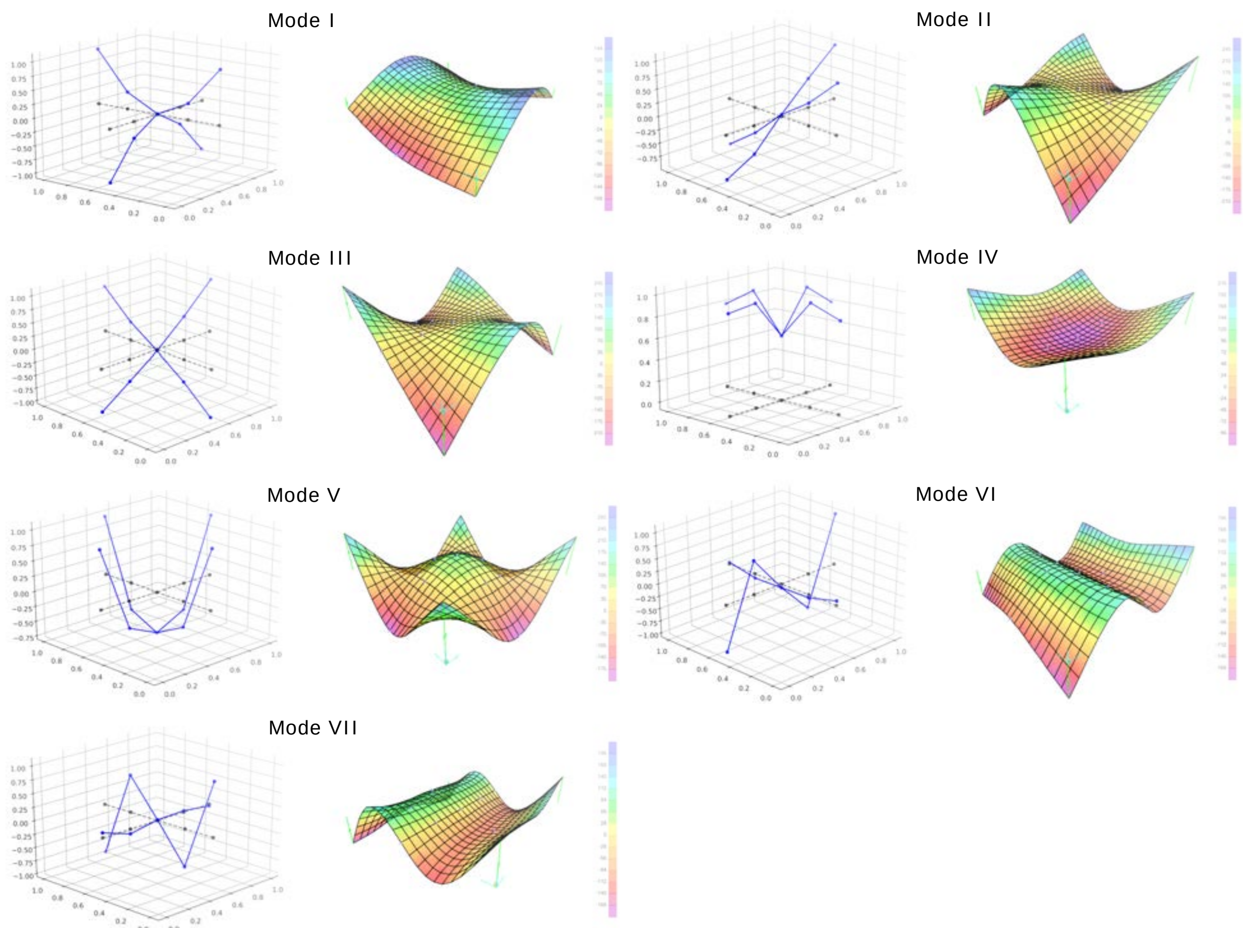

Fig. 8. Experimental and numerical mode shapes of the plywood board.

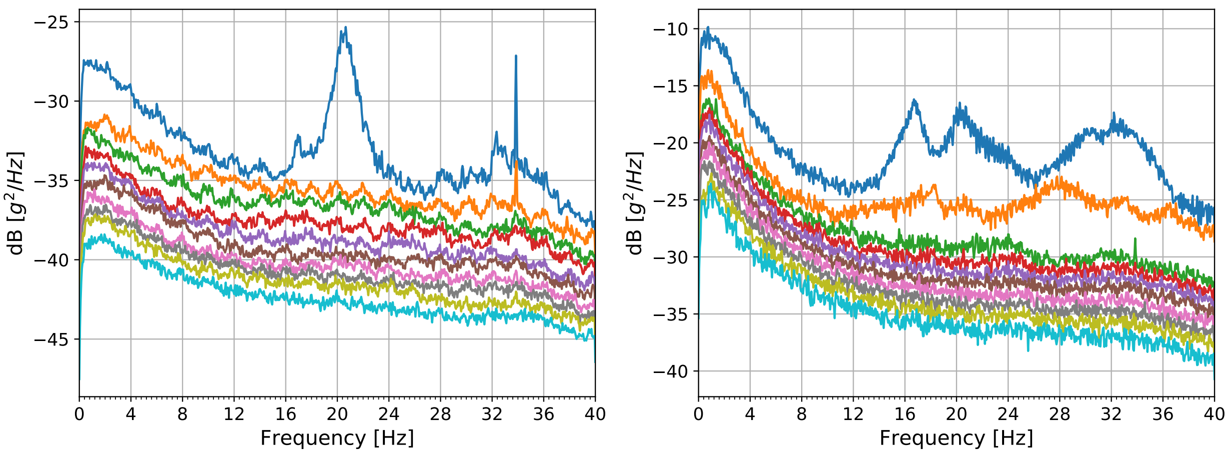

Fig. 9. Singular values plot: left unexcited floor, right excited floor.

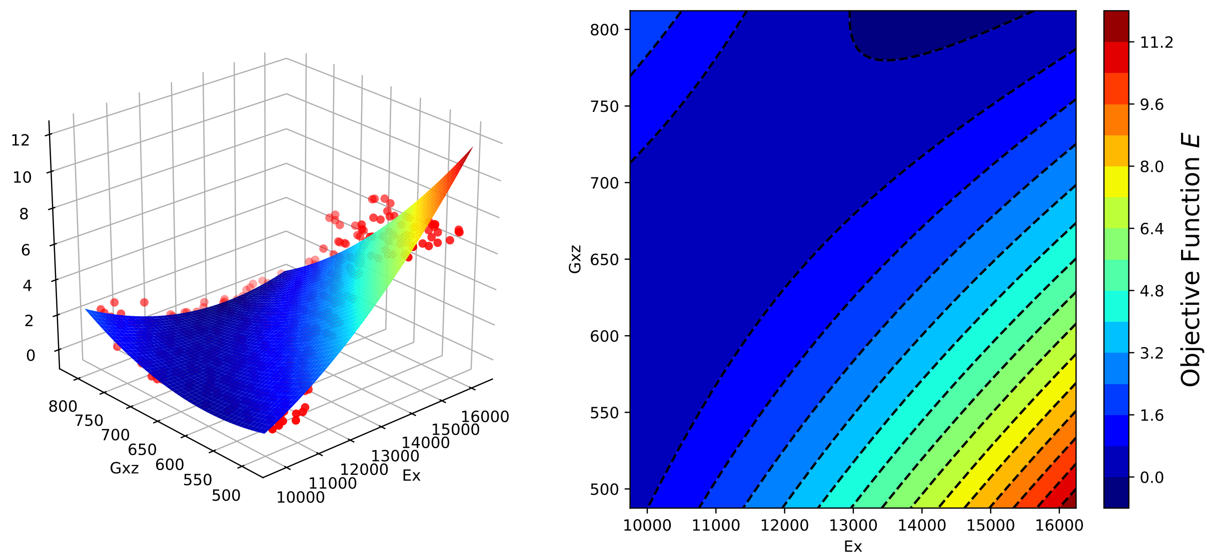

Fig. 10. 2^{nd} order polynomial fit: left 3D view with data points, right contour plot.